Published OnlineFirst May 9, 2011; DOI: 10.1158/0008-5472.CAN-10-4610

Cancer Research

Targeting Hyaluronidase for Cancer Therapy: Antitumor Activity of Sulfated Hyaluronic Acid in Prostate Cancer Cells

Anaid Benitez[1], Travis J. Yates[3], Luis E. Lopez[1], Wolfgang H. Cerwinka[1], Ashraf Bakkar[1], and Vinata B. Lokeshwar[1,2,3]

Abstract

The tumor cell–derived hyaluronidase (HAase) HYAL-1 degrades hyaluronic acid (HA) into proangiogenic fragments that support tumor progression. Although HYAL-1 is a critical determinant of tumor progression and a marker for cancer diagnosis and metastasis prediction, it has not been evaluated as a target for cancer therapy. Similarly, sulfated hyaluronic acid (sHA) has not been evaluated for biological activity, although it is an HAase inhibitor. In this study, we show that sHA is a potent inhibitor of prostate cancer. sHA blocked the proliferation, motility, and invasion of LNCaP, LNCaP-AI, DU145, and LAPC-4 prostate cancer cells, and induced caspase-8–dependent apoptosis associated with downregulation of Bcl-2 and phospho-Bad. sHA inhibited Akt signaling including androgen receptor (AR) phosphorylation, AR activity, nuclear factor κB (NFκB) activation, and VEGF expression. These effects were traced to a blockade in complex formation between phosphoinositide 3-kinase (PI3K) and HA receptors and to a transcriptional downregulation of HA receptors, CD44, and RHAMM, along with PI3K inhibition. Angiogenic HA fragments or overexpression of myristoylated Akt or HA receptors blunted these effects of sHA, implicating a feedback loop between HA receptors and PI3K/Akt signaling in the mechanism of action. In an animal model, sHA strongly inhibited LNCaP-AI prostate tumor growth without causing weight loss or apparent serum-organ toxicity. Inhibition of tumor growth was accompanied by a significant decrease in tumor angiogenesis and an increase in apoptosis index. Taken together, our findings offer mechanistic insights into the tumor-associated HA–HAase system and a preclinical proof-of-concept of the safety and efficacy of sHA to control prostate cancer growth and progression. *Cancer Res; 71(12); 4085–95.* ©*2011 AACR.*

Introduction

Tumor-associated hyaluronic acid (HA) and hyaluronidase (HAase) system is known to promote tumor growth and metastasis (1). HA is a nonsulfated glycosaminoglycan that is elevated in tumor tissues (2–7). Although HA synthesis is mediated by HA synthases (HAS1, HAS2, and HAS3), cellular effects of HA are mediated through HA receptors, CD44 and RHAMM. HA–HA receptor interaction generates intracellular signaling, which, in turn, promotes tumor growth, metastasis, angiogenesis, trafficking of tumor-associated macrophages, and chemoresistance (8–14). Our recent work shows that 4-methylumbelliferone (4-MU), an HA synthesis inhibitor, has antitumor activity in prostate cancer cells (15).

The other component in the tumor-associated HA–HAase system is HYAL-1, a tumor cell-derived HAase. HYAL-1 at levels expressed in tumor cells and tissues promotes tumor growth, invasion, and angiogenesis in prostate and bladder cancer models (16, 17). Furthermore, HA synthase expression requires HYAL-1 to promote tumor growth and progression (18, 19). HYAL-1 expression is potentially an independent predictor of metastasis (3, 6, 20, 21). Although HYAL-1 is a molecular determinant of cancer growth and progression, so far no study has targeted it for cancer therapy.

Sulfated hyaluronic acid (sHA), generated by O-sulfation of HA, was shown to inhibit both urinary and testicular HAases 60 years ago (22). We have shown that sHA polymers such as sHA2.75, in which 75% of HA oligosaccharides contain 3-sulfate groups and 25% contain 2-sulfate groups, are potent inhibitors of HYAL-1 activity (23). sHA2.75 inhibits HAase activity through a mixed inhibition mechanism (i.e., competitive + uncompetitive) and it is 15-fold better as an uncompetitive inhibitor than as a competitive inhibitor.

Authors' Affiliations: Departments of [1]Urology and [2]Cell Biology and Anatomy, and [3]Sylvester Comprehensive Cancer Center, University of Miami Miller School of Medicine, Miami, Florida

Note: Supplementary data for this article are available at Cancer Research Online (http://cancerres.aacrjournals.org/).

A. Benitez, T.J. Yates, and L.E. Lopez contributed equally and are joint first authors.

Current address for W.H. Cerwinka: Georgia Pediatric Urology, Children's Healthcare of Atlanta, Emory University, 5445 Meridian Mark Rd., Ste. 420, Atlanta, GA 30342.

Current address for A. Bakkar: Department of Pathology and Lab Medicine, Tom Baker Cancer Centre, Translational Labs AGE88, University of Calgary, 1331 29 St NW, Calgary, Alberta, Canada T2N 4N2.

Corresponding Author: Vinata B. Lokeshwar, Department of Urology (M-800), University of Miami Miller School of Medicine, P.O. Box 016960, Miami, FL 33101. Phone: 305-243-6321; Fax: 305-243-6893; E-mail: vlokeshw@med.miami.edu

doi: 10.1158/0008-5472.CAN-10-4610

Published OnlineFirst May 9, 2011; DOI: 10.1158/0008-5472.CAN-10-4610

sHA polymers have been shown to affect proliferation of osteoblasts, gene expression in keratinocytes and astrocytes, and adhesion and motility in fibroblasts (24–26). However, antitumor activity of sHA compounds has not been explored. In this study, we evaluated the antitumor activity of sHA and the molecular mechanism associated with such activity.

Materials and Methods

Cell culture

Cell lines LNCaP, DU145, and RWPE-1 (immortalized normal adult prostate epithelial cells) were obtained from American Type Culture Collection (ATCC) and cultured in RPMI 1640 + 10% FBS + gentamicin. LAPC-4 cells kindly provided by Dr. Charles Sawyer (Memorial Sloan Kettering Cancer Center, New York, NY) were maintained in Iscove's medium with 7.5% FBS and 1 nmol/L dihydrotestosterone. C4-2 and C4-2B cells were obtained from Viromed Laboratories and cultured in T-Medium + 10% FBS + gentamicin. LNCaP-AI (LNAI) is a spontaneously derived androgen-independent subline of LNCaP. LNAI cells express androgen receptor (AR) and prostate-specific antigen (PSA) in a manner similar to LNCaP (27). The presence of dihydrotestosterone did not increase the growth of LNAI cells (Supplementary Fig. S1A). Cell lines were authenticated by Genetica DNA Laboratories Inc.; further in-house characterization is presented in Supplementary Table S2. These authentications were carried out during the course of this work.

Reagents

sHA was prepared from tributylamine salt of HA (molecular weight 320–490 kDa; Genzyme Corp.; ref. 23). Antibodies, constructs, and reagents used in this study are described in Supplementary Information.

Cell proliferation and apoptosis

Prostate cancer cells [$(1.5–2.0) \times 10^4$ cells/well] cultured in growth medium were exposed to sHA (0–40 μg/mL) and counted every 24 hours or after 48 to 72 hours. In some experiments, HA12K or HA8K (average molecular weight 12 and 8 kDa, respectively), caspase-8 inhibitor IETD-CHO (5 μmol/L), or LY29400 was added to the wells at the time of sHA addition. For apoptosis assay, cells were treated with sHA and apoptosis was analyzed after 48 hours by using the Cell Death ELISA Plus Kit. Apoptosis index was calculated as optical density $(OD)_{450\ nm}$ per 20,000 cells. LNAI cells were also treated with sHA for 24 hours, and cell-cycle analysis was conducted as described previously (16).

Motility and invasion assays

Matrigel invasion and motility assays were carried out as described previously (15–17) except that sHA was added in both chambers of the Transwell (see Supplementary Information).

Immunoblot analyses, time course, and VEGF ELISA

Prostate cancer cells (40,000–50,000 cells/6-well plate) were exposed to sHA (0–10 μg/mL) for 48 hours. For time course experiments, 8- to 12-hour cultures of LNAI cells were exposed to sHA (5 μg/mL) for 3, 6, 12, and 24 hours. In some wells, 50 μg/mL HA12K was added at the time of sHA addition. Cell lysates (~20,000-cell equivalent) were immunoblotted using specific antibodies; β-actin and PPIA4 [peptidylprolyl isomerase A (cyclophilin A)] were used as loading controls. For VEGF ELISA, serum-free conditioned media (16, 17) from control and sHA-treated LNAI cells were assayed for VEGF levels by using an ELISA kit.

HAase activity assay

Serum-free conditioned media of LNAI and DU145 cells were subjected to HAase ELISA-like assay in the presence of sHA (0–40 μg/mL). The HAase activity was normalized to units $\times 10^{-4}/10^6$ cells, as described before (23).

Immunoprecipitation and phosphoinositide 3-kinase activity assay

LNAI and DU145 cells treated with sHA were immunoprecipitated using a rabbit anti-p85 phosphoinositide 3-kinase (PI3K) subunit antibody or rabbit IgG. The immunoprecipitates were either subjected to immunoblotting using a mouse anti-CD44, anti-RHAMM, or anti-p85 PI3K antibody or subjected to PI3K activity assay (see Supplementary Information).

Transient transfection assays

LNAI and DU145 cells were transiently transfected with myr-HA-Akt1 plasmid (myr-Akt), pcDAN3.1-RHAMM, or pcDNA3.1-CD44 (standard form, CD44s) expression plasmids or vector. Alternatively, cells were transfected with control siRNA or CD44 and/or RHAMM siRNA (50 nmol/L each; ref. 15). Twenty-four hours following transfection, the cells were exposed to sHA and analyzed after 48 hours for proliferation, apoptosis, and protein and gene expression (see Supplementary Information). For nuclear factor κB (NF&KAPPA;B) and PSA reporter assays, vector and myr-Akt transfectants were transiently transfected with pNFκB-Luc or PSAe1p/Luc plasmid (28).

Quantitative reverse transcription-PCR assays

Transient transfectants or prostate cancer cells treated with sHA ± HA12K were subjected to quantitative reverse transcription-PCR (qRT-PCR), using the iQ SYBR Green Supermix and the primers described in Supplementary Table S1. mRNA levels were normalized to peptidylprolyl isomerase A (PPIA4 mRNA levels; ref. 15).

Tumor xenografts

LNAI cell suspension (2×10^6 cells/0.1 mL) was mixed 1:1 with Matrigel and implanted subcutaneously on the dorsal flank of 5- to 6-month-old athymic mice. In the first experiment, there were 4 mice in each group, vehicle (PBS), sHA 25 mg/kg, sHA 50 mg/kg. sHA was injected intraperitoneally twice weekly. The treatment began on the day of injection. Animals in the control group were euthanatized on day 29 and on day 40 in the sHA 25 mg/kg group. In the sHA 50/kg group, 3 mice were euthanatized on day 40 and the remaining on day 64 after stopping the treatment on day 50. Tumor volume was measured twice weekly. In a second experiment, there

Published OnlineFirst May 9, 2011; DOI: 10.1158/0008-5472.CAN-10-4610

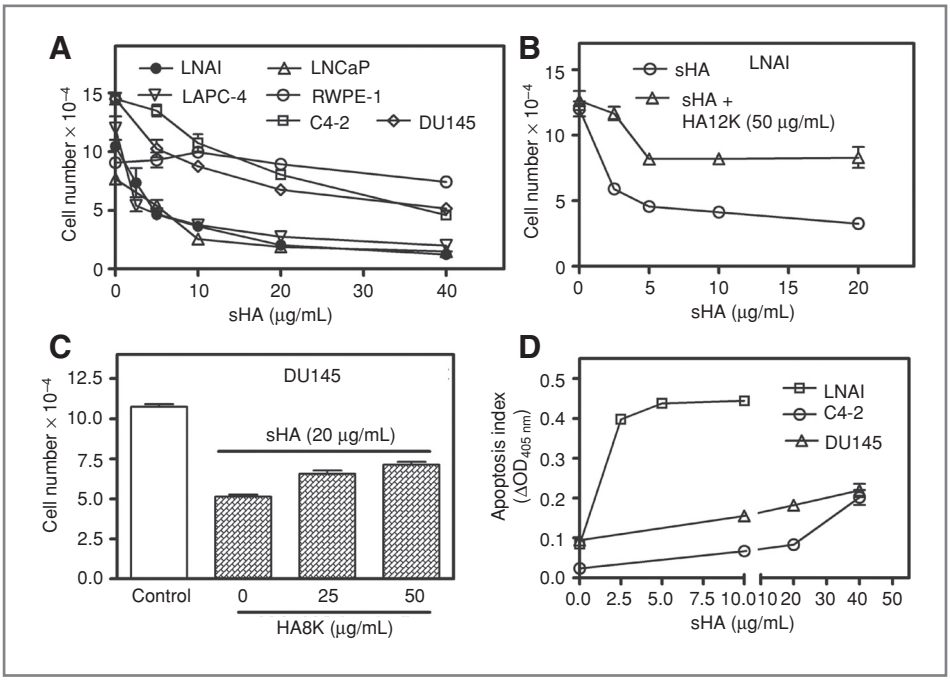

Figure 1. Effect of sHA on cell proliferation. A, cell-counting data at 72 hours following treatment with sHA. LNAI (B) and DU145 (C) cells were treated with sHA + 50 μg/mL of HA8K or HA12K and counted after 72 hours. Data: mean ± SD. D, measurement of apoptosis in cells treated with sHA for 48 hours. Data: mean ± SD.

were 5 animals in the control and 10 animals in the sHA 50 mg/kg group. In the sHA 50 mg/kg group, 5 animals were euthanatized on day 42 and 5 mice were left untreated from day 53 to day 70. Tumors or the Matrigel sac (if visible) was fixed for immunohistochemistry [to localize microvessels or terminal deoxynucleotidyl transferase–mediated dUTP nick end labeling (TUNEL)-positive cells; refs. 15–17] and histopathology (conducted at Charles River Laboratories). Microvessel density (MVD) and TUNEL assays are described in the Supplementary section. Serum chemistry analysis and histopathologic evaluation of kidney, lung, and liver were conducted by the Division of Comparative Pathology, University of Miami.

Determination of serum sHA levels

Fourteen-week-old athymic mice (average weight ~30 g) were injected intraperitoneally with sHA (86.7 mg/kg). At various time intervals, mice were euthanatized and serum was assayed for uronate levels (total glycosaminoglycan) by a modified uronic carbazole assay established by Bitter and Müir (29). Serum sulfated glycosaminoglycan levels were measured using Farndale's dimethylmethylene blue assay (29). We have previously used these assays to measure urinary glycosaminoglycan and sulfated glycosaminoglycan levels (29). We have previously shown the detection of sHA by Farndale's assay (23).

Results

sHA inhibits HAase activity and cell proliferation in prostate cancer cells

We have previously shown that LNCaP and DU145 cells express 5- to 10-fold more HAase activity than PC3-ML cells and that HYAL-1 is the only HAase expressed in prostate cancer cells (7, 30). Furthermore, consistent with our previous results, sHA inhibited the HAase activity secreted in the conditioned media of LNAI and DU145 cells in a dose-dependent manner (Supplementary Fig. S1B). sHA did not affect HYAL-1 expression, as determined by qRT-PCR (data not shown). As shown in Figure 1A, sHA inhibited the growth of all prostate cancer cell lines but not of prostate epithelial cells (RWPE-1). The IC_{50} value for LNCaP, LNAI, and LAPC-4 cells was 5 to 10 μg/mL, whereas for DU145 and C4-2 cells it was 20 to 40 μg/mL. At IC_{50} or at higher values, the differences in cell numbers between untreated and sHA-treated samples were statistically significant ($P \leq 0.005$; unpaired t-test). Time course experiment showed that sHA inhibited the growth of LNAI cells at each time point (Supplementary Fig. S1C). To determine whether the antiproliferative effect of sHA was due to the inhibition of HAase activity, we treated LNAI and DU145 cells with sHA in the presence of angiogenic HA fragments, which are generated because of the degradation of HA by HAase. As shown in Figure 1B, in LNAI cells, HA12K partially reversed the growth inhibition by sHA (64% inhibition at 5 μg/mL sHA; 36% inhibition at 5 μg/mL sHA + HA12K). This partial reversal was independent of the average molecular weight of HA fragments, because HA8K showed a similar effect on the growth inhibition by sHA in DU145 cells (Fig. 1C).

sHA induces apoptosis in prostate cancer cells

To examine why sHA inhibits cell growth, we conducted cell-cycle analysis. As shown in Supplementary Figure S1D, sHA induced approximately 20% increase G_0–G_1 phase with a corresponding decrease in G_2–M and S-phases. However, the cytotoxic effect of sHA was more likely mediated by its ability to induce apoptotic cell death; at IC_{50}, the increase in apoptosis was 200% in DU145 and C4-2 and 500% in LNAI cells, respectively (Fig. 1D). Because apoptosis induction

Published OnlineFirst May 9, 2011; DOI: 10.1158/0008-5472.CAN-10-4610

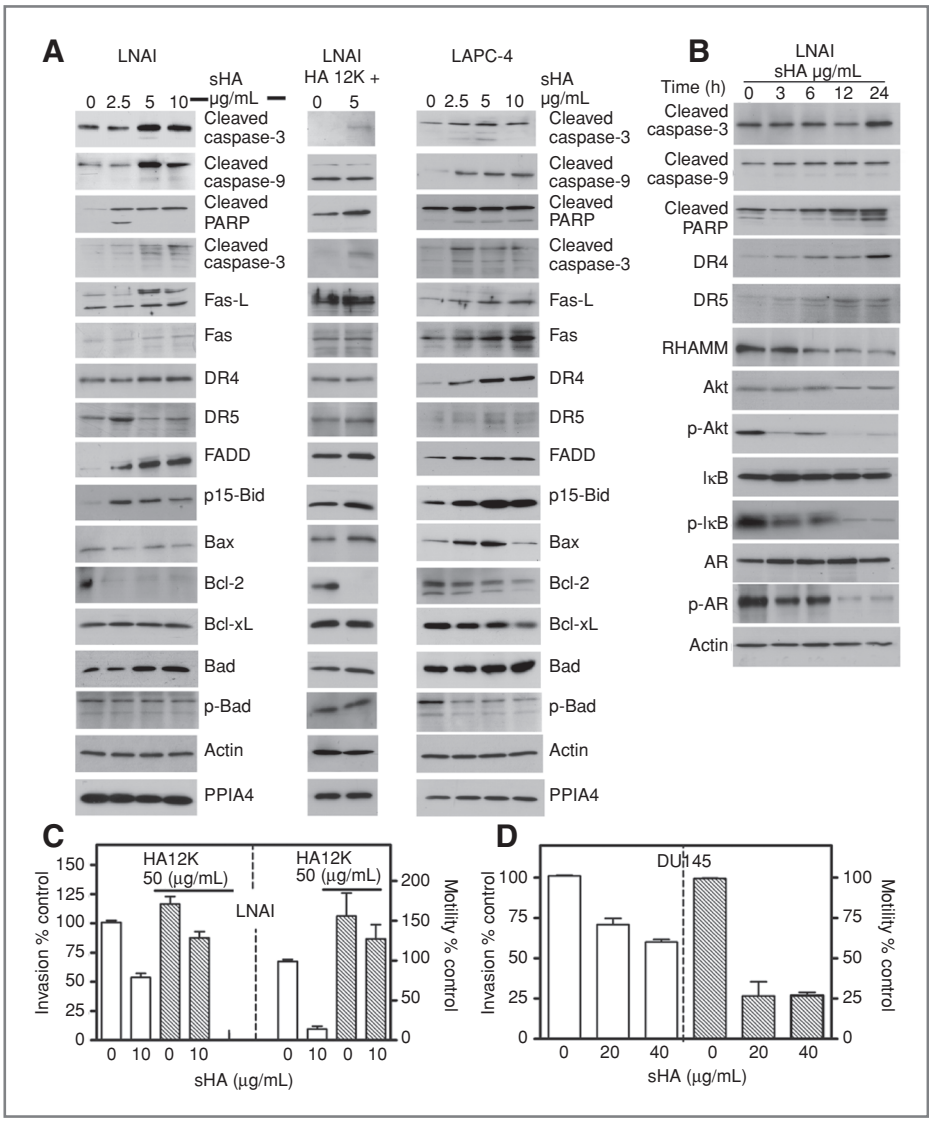

Figure 2. Effect of sHA on apoptosis, invasion, and chemotactic motility. A, LNAI and LAPC-4 cells were treated with sHA in the presence (LNAI cells, middle) or absence of HA12K for 48 hours and subjected to immunoblot analyses for apoptosis-related proteins. B, LNAI cells were treated with sHA (5 μg/mL) for the indicated time periods and subjected to immunoblot analyses. phospho-Akt, p-Akt; phospho-IκB, p-IκB; phospho-AR, p-AR. Determination of invasive activity and chemotactic motility of LNAI (C) and DU145 (D) cells treated with sHA and/or HA12K. Data: mean ± SD.

was substantial, we investigated its mechanism. In LNAI and LAPC-4 cells, sHA induced the activation of proapoptotic effectors (caspase-3, caspase-9, and caspase-8; 2- to 5-fold), PARP cleavage and upregulation of death receptor signaling complex proteins (Fas, Fas-L, DR4, DR5, FADD, and Bid cleavage) in a dose-dependent manner (Fig. 2A). The upregulation of proapoptotic effectors and death receptors was observed as early as 6 to 12 hours after the exposure of LNAI cells to sHA (Fig. 2B). In both LNAI and LAPC-4 cells, sHA also downregulated Bcl-2 and phosphorylated Bad levels, without significantly affecting Bcl-xL, Bax, and total Bad levels. Except for Fas, DR4, phospho-Bad (p-Bad), and DR5 levels, the addition of HA12K during sHA incubation, either did not prevent (caspase-3, caspase-8, and Bcl-2) or partially prevented (PARP, Fas-L, and p15-Bid) the effect of sHA on apoptosis effectors. When LNAI cells were incubated with sHA in the presence of a cell-permeable caspase-8 inhibitor, IETD-CHO, both growth inhibition and sHA-induced apoptosis were significantly attenuated (Supplementary Fig. S1E), suggesting the involvement of the extrinsic pathway in sHA-induced apoptosis.

sHA inhibits chemotactic motility and invasion

Because HYAL-1 promotes tumor invasion and metastasis (18–21), we investigated whether sHA inhibits chemotactic motility and invasive potential of prostate cancer cells. As shown in Figure 2C and D, sHA caused 75% or more inhibition of chemotactic motility in both LNAI and DU145 cells ($P \leq 0.0001$; unpaired t-test). HA12K caused 150% increase in the motility of LNAI cells and reduced the sHA-induced inhibition of motility by 80%. Similarly, sHA inhibited the invasive activity of LNAI and DU145 cells by 40% to 50% ($P < 0.001$; unpaired t-test); in LNAI cells, HA12K reduced this inhibition by more than 80%. Therefore, sHA inhibits chemotactic motility and invasion plausibly by inhibiting HAase activity.

Published OnlineFirst May 9, 2011; DOI: 10.1158/0008-5472.CAN-10-4610

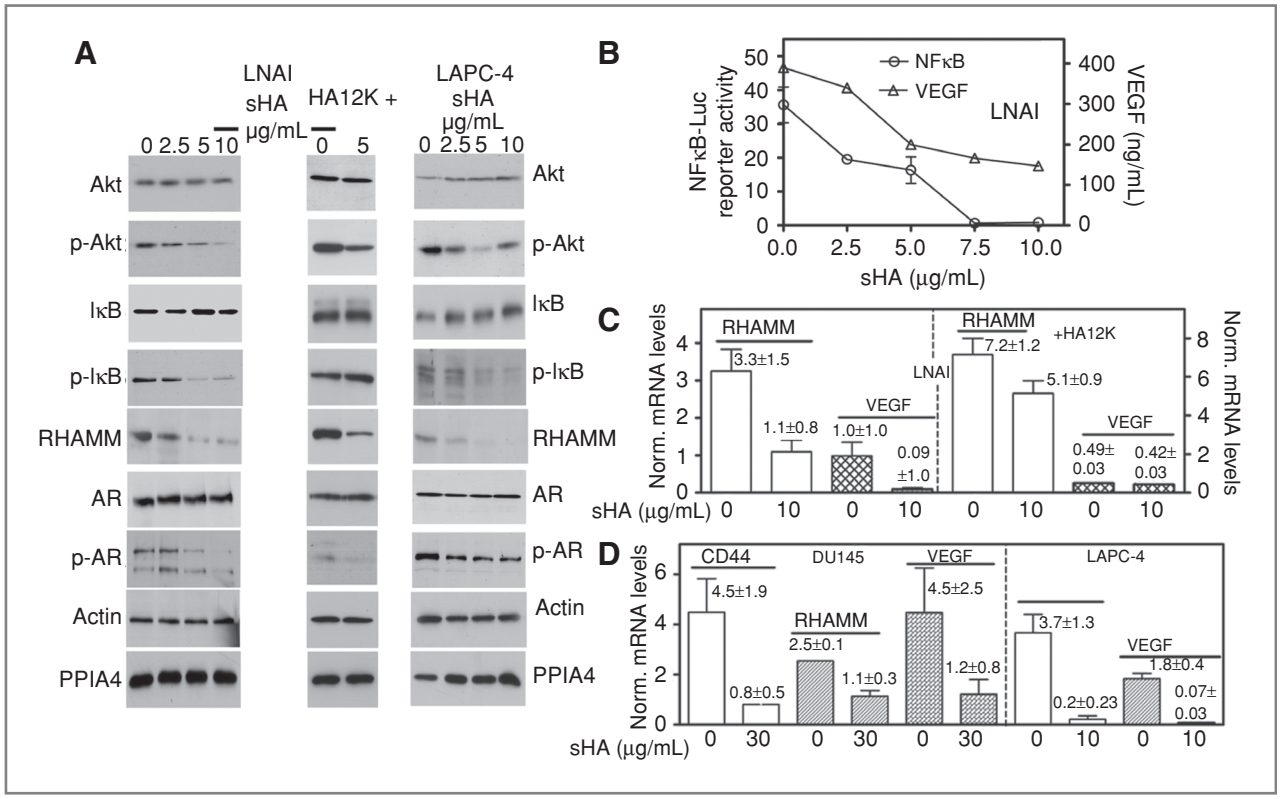

Figure 3. Effect of sHA on Akt signaling and HA receptor expression. A, LNAI and LAPC-4 cells were treated with sHA in the presence (LNAI cells, middle) or absence of HA12K for 48 hours and subjected to immunoblot analyses. phospho-Akt, p-Akt; phospho-IκB, p-IκB; phospho-AR, p-AR. B, LNAI cells transfected with pNFκB-Luc reporter construct were treated with sHA and the luciferase activity was measured (left axis). LNAI cells were treated with sHA for 48 hours and the conditioned medium was assayed for VEGF (right axis). Data: mean ± SD. C and D, prostate cancer cells were treated with sHA for 48 hours and HA receptor and VEGF mRNA levels were measured by qRT-PCR. Alternatively, LNAI cells were incubated with both sHA and HA12K and assayed for VEGF.

sHA inhibits Akt signaling

Because Bad is phosphorylated by Akt at Ser136 and sHA downregulates phosphorylated Bad levels, we investigated whether sHA inhibits Akt activation. As shown in Figure 3A, sHA downregulated phosphorylated Akt levels (>3-fold decrease at 5–10 μg/mL) in both LNAI and LAPC-4 cells and this decrease was partially prevented by HA12K. Akt activates NFκB by phosphorylating IκB kinase α (IKKα), which, in turn, phosphorylates IκB, targeting it for degradation. As shown in Figure 3A, sHA decreased phosphorylated IκB levels in both LNAI and LAPC-4 cells and the addition of HA12K prevented this decrease. As expected sHA inhibited NFκB promoter luciferase reporter activity (Fig. 3B). At 7.5 μg/mL, sHA caused approximately 100% inhibition of NFκB reporter activity (35.6 ± 10.6 vs. 0.67 ± 0.32; $P < 0.0001$). NFκB activation induces VEGF expression (31). As shown in Figure 3B, sHA decreased VEGF levels secreted in the conditioned medium of LNAI cells in a dose-dependent manner.

The PI3K/Akt signaling pathway regulates AR activity by phosphorylating AR at Ser210/213 and Ser791/790 (32–34). sHA inhibited AR phosphorylation on Ser210/213 in both LNAI and LAPC-4 cells; however the addition of HA12K did not prevent the decrease in phosphorylated AR levels (Fig. 3A). The time course of the decrease in phosphorylated Akt, IκB, and AR levels followed the same pattern; a decrease was observed in as early as 3 hours and the levels decreased by more than 80% after 12 hours of incubation (Fig. 2B).

sHA transcriptionally downregulates HA receptor and VEGF expression

Angiogenic HA fragments induce CD44 expression and cellular signaling through both CD44 and RHAMM (35–37). sHA treatment downregulated RHAMM levels in a dose-dependent manner in both LNAI and LAPC-4 cells (Fig. 3A). RHAMM downregulation was observed within 6 hours of sHA treatment (Fig. 2B), and it was not effectively prevented by HA12K (Fig. 3A). sHA also downregulated RHAMM and VEGF mRNA levels by 3-fold and 100-fold, respectively, in LNAI cells (Fig. 3B). Addition of HA12K partially (RHAMM) or completely (VEGF) prevented the observed decrease in these transcripts (Fig. 3C). In LAPC-4 cells, sHA downregulated RHAMM and VEGF transcript levels by 18.5- and 25.7-fold, respectively (Fig. 3D).

With the exception of a derivative CL1, LNCaP cell line and its derivatives (e.g., C4-2 and C4-2B), and LAPC-4 cells do not express CD44 because of promoter hypermethylation (38–45). We also did not observe CD44 expression [standard (CD44s) and variant (CD44v) isoform(s)] in these cells (Supplementary Table S2). Two publications have reported CD44 expression in LNCaP and C4-2 cells (46, 47), including the expression of a

Published OnlineFirst May 9, 2011; DOI: 10.1158/0008-5472.CAN-10-4610

CD44 variant, CD44-v9 (46). However, no PCR product was amplified from LNCaP, LNAI, LAPC-4, C4-2, and C4-2B cells, using the same PCR primer pair that was used to amplify CD44-v9 (46, 48). A 632-base PCR product (CD44-epithelial isoform) was amplified from PC3-ML and DU145 cells which included exon v9 (exon 13), exon v10 (exon 14), and common exons 15 to 17 (Supplementary Fig. S2A). The expression of CD44s transcript was 26- and 49-fold higher than that of CD44v transcript in DU145 and PC3-ML cells, respectively (Supplementary Table S2). In DU145 cells, sHA caused 5.6- and 2.5-fold decrease in CD44 (data shown for CD44s) and RHAMM mRNA levels, respectively, and a 4-fold decrease in VEGF levels (Fig. 3D).

sHA inhibits PI3K activity and complex formation between HA receptors and PI3K

sHA-mediated inhibition of Akt phosphorylation suggested that sHA might be either inhibiting the activity of PI3K or accelerating dephosphorylation of phosphatidylinositol-3,4,5-trisphosphate (PIP3) by PTEN. Because sHA downregulated Akt phosphorylation in PTEN-positive (DU145) and PTEN-negative (LNAI and LAPC-4) cells, we investigated whether sHA inhibited PI3K activity. As shown in Supplementary Figure S2B and C, there was no difference in the amount of PI3K (p85 subunit) immunoprecipitated from the control and sHA-treated LNAI and DU145 cells; however, the PI3K activity was significantly inhibited in sHA-treated samples. Furthermore, although both CD44 and RHAMM were coimmunoprecipitated with the p85 subunit in untreated samples, their amount was significantly reduced in immunoprecipitates from sHA-treated samples. Treatment of LNAI cells with LY29400, a PI3K inhibitor, and sHA synergistically inhibited cell growth (Supplementary Fig. S2D). The combination index (CI) calculated by Chou–Talalay analysis (Calcusyn; Biosoft Inc.) was 0.017, suggesting strong synergy. These results showed that sHA decreased Akt signaling by inhibiting PI3K activity.

Combined effect of HA receptor downregulation and sHA treatment on prostate cancer cells

Because both HA and angiogenic HA fragments signal through HA receptors, we examined whether downregulation of CD44 and/or RHAMM mimics sHA effects. In DU145 cells, sHA downregulated RHAMM and CD44 protein (Fig. 4A) and mRNA expression (~6-fold; Supplementary Fig. S3). RHAMM and CD44 siRNAs downregulated RHAMM and CD44 protein expression, respectively (RHAMM, CD44, and CD44 + RHAMM panels, Fig. 4A). Addition of sHA did not further decrease HA receptors levels plausibly because the siRNAs decreased the levels of respective transcripts by more than 30-fold (Supplementary Fig. S3). RHAMM protein and mRNA were not detectable when LNAI cells were treated with both sHA and RHAMM siRNAs (Fig. 4A and Supplementary Fig. S3).

In DU145 cells, downregulation of RHAMM or CD44 decreased phosphorylated Akt levels; however, sHA was more effective. sHA and CD44 + RHAMM siRNAs caused more than 5-fold decrease in phosphorylated Akt levels. In LNAI cells, both sHA and RHAMM siRNA caused more than 50% decrease in phosphorylated Akt levels, and their combination caused more than 80% decrease (Fig. 4A).

Both sHA and HA receptor siRNA treatments decreased cell growth. However, the combination of sHA and CD44 + RHAMM siRNAs caused a 5.1-fold inhibition of cell growth and a 4.4-fold increase in apoptosis in DU145 cells (Fig. 4B; $P < 0.0001$; unpaired t-test). In LNAI cells, sHA and RHAMM siRNA combination inhibited LNAI cell growth by 5-fold and increased apoptosis by approximately 9-fold (Fig. 4C; $P < 0.0001$; unpaired t-test). Chou–Talalay analysis showed a synergistic effect of sHA and HA receptor siRNA treatments on growth inhibition. The CI for each combination to inhibit the growth of DU145 cells was as follows: sHA + CD44 siRNA: 0.143; sHA + RHAMM siRNA: 0.102; sHA + (CD44 + RHAMM) siRNA: 0.051. In LNAI cells, the CI for sHA + RHAMM siRNA was 0.082. In DU145 cells, HA receptor downregulation or sHA caused a 5- to 10-fold decrease in VEGF mRNA levels and, when both were combined, VEGF mRNA levels were undetectable. In LNAI cells, both sHA and RHAMM siRNAs completely downregulated VEFG mRNA levels (Fig. 4D). Conversely, overexpression of CD44, RHAMM, or CD44 + RHAMM in LNAI cells attenuated sHA-induced growth inhibition; growth inhibition in transfectants at 5 μg/mL: vector: 64.4%; RHAMM: 20%; CD44: 12%; CD44 + RHAMM: 20% (Supplementary Fig. S4C). Similar results were observed with respect to VEGF downregulation by sHA (data not shown).

Effect of constitutive Akt activation on sHA-induced cellular effects

Because Akt activation was downregulated by both sHA and HA receptor siRNA treatments, we investigated various effects of sHA in LNAI cells transfected with myristoylated Akt plasmid (myr-Akt). As shown in Figure 5A, myr-Akt transfection increased total Akt and phosphorylated Akt levels by more than 10-fold. sHA treatment did not downregulate phosphorylated Akt, phosphorylated IκB, phosphorylated AR, and RHAMM levels in myr-Akt transfectants. myr-Akt expression also attenuated the effect of sHA on cell proliferation, apoptosis, caspase-8 activation, and Fas-L upregulation (Fig. 5A and B). myr-Akt expression caused a 4-fold increase in NFκB reporter activity and prevented the sHA-mediated decrease in NFκB transcriptional activity (Fig. 5C). Similarly, myr-Akt reversed the effect of sHA on PSA promoter activity and downregulation of VEGF transcript levels (Fig. 5C and D).

Effect of sHA on tumor growth and angiogenesis

Effect of sHA treatment on LNAI xenografts is shown in Figure 6A. sHA significantly inhibited tumor growth at 25 and 50 mg/kg doses. On day 29, the average tumor volumes in the vehicle group (1,191.1 ± 299.5 mm^3) were significantly higher than in sHA 25 mg/kg (176.1 ± 105 mm^3) and sHA 50 mg/kg (0.143 ± 0.01 mm^3); $P < 0.001$ (Tukey's multiple comparison test). The tumors in the vehicle group were vascular and hemorrhagic (Fig. 6B). The experiment was terminated on day 40 in the sHA 25 mg/kg group (mean tumor volume = 385 ± 263 mm^3). Only one animal developed a palpable tumor by day 40 in the sHA 50 mg/kg group; 8 of 14 animals were euthanized after 39 to 42 days. In the remaining 6 animals,

Published OnlineFirst May 9, 2011; DOI: 10.1158/0008-5472.CAN-10-4610

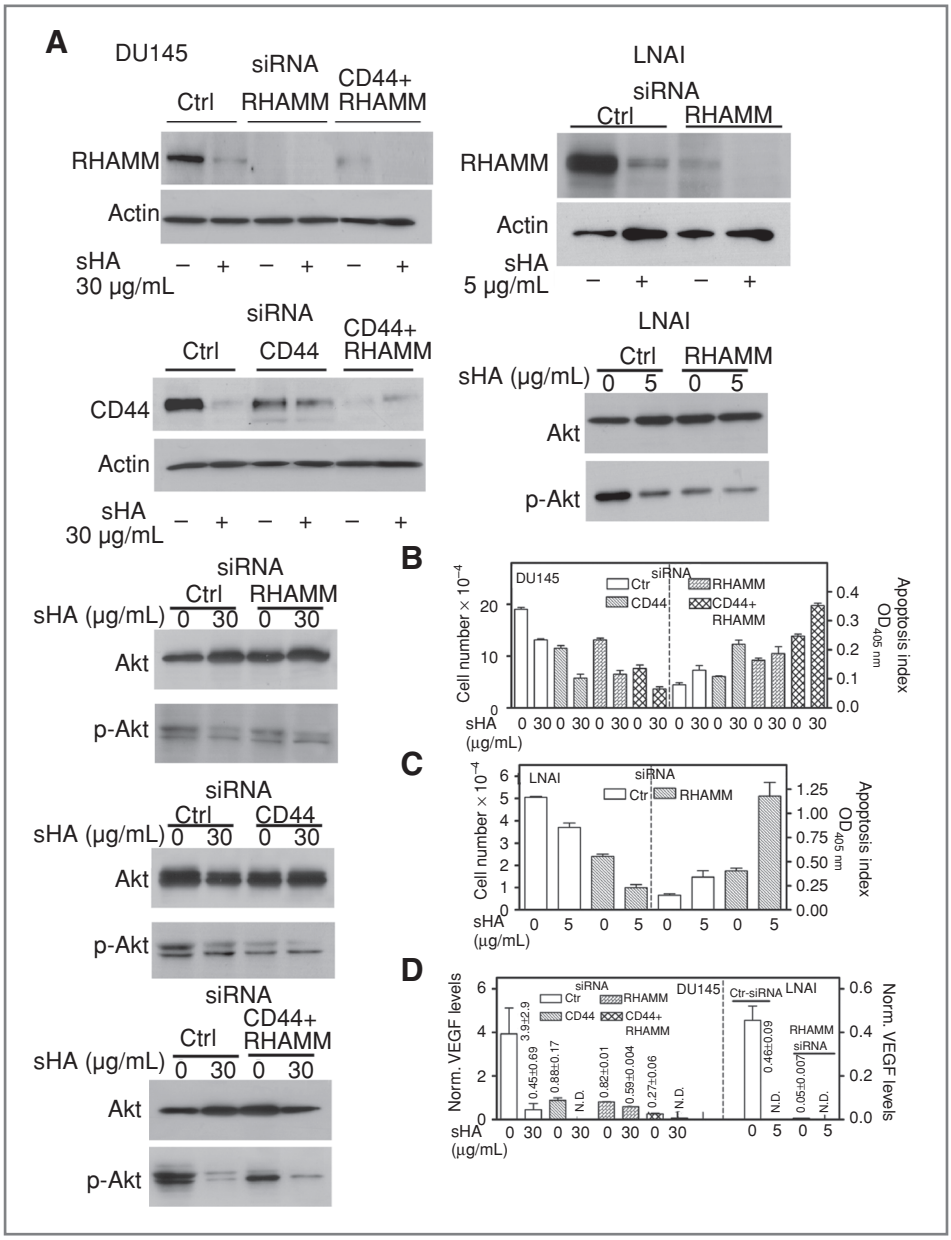

Figure 4. Effect of sHA and CD44 + RHAMM siRNA treatment on LNAI and DU145 cells. DU145 and LNAI cells were transfected with CD44 and/or RHAMM siRNA followed by sHA treatment. A, immunoblot analysis of transfectants for HA receptors, Akt, and phosphorylated Akt. phospho-Akt, p-Akt. 48 hours following sHA treatment, the DU145 (B) and LNAI (C) transfectants were counted in duplicate (left) or subjected to the measurement of apoptosis in triplicate (right). Data: mean ± SD. D, measurement of VEGF mRNA levels by qRT-PCR. Data: mean ± SD.

treatment was stopped for 1 animal on day 50 until day 63 and this animal did not develop tumor. For 5 animals, treatment was stopped from day 53 until day 70. As shown in Figure 6A, the mean tumor volume at day 70 was 249 ± 192 mm^3; only 2 animals developed a tumor. There was no decrease in the weight of sHA-treated animals and the animals gained weight (Supplementary Fig. S4). Evaluation of fixed kidney, liver, and lung tissues revealed no organ toxicity in sHA-treated animals (Supplementary Fig. S5B), which was further confirmed by serum chemistry analysis (Supplementary Table S3).

The serum half-life of sHA was determined by measuring serum uronate (total glycosaminoglycan) and sulfated glycosaminoglycan levels. As shown in Figure 6C, following sHA administration, there was an increase in both serum uronate and sulfated glycosaminoglycan levels; peak levels were achieved at 6 hours following intraperitoneal injection. The serum half-life of sHA in circulation was approximately 24 hours.

Tumor histology showed that tumors in the vehicle group formed larger masses and had clear evidence of the formation of fibrovascular stroma (Fig. 6B). Contrarily, the Matrigel sac removed from the injection site in the sHA 50 mg/kg group (day 39), consisted primarily of groups of tumor cells still embedded in the Matrigel without clear evidence of neovascularization. Tumor cells in the sHA-treated group were degenerate, some with small dark (pyknotic) or fragmented (karyorrhectic) nuclei. Tumor cells present in the Matrigel sac in sHA 50 mg/kg group were apoptotic

Published OnlineFirst May 9, 2011; DOI: 10.1158/0008-5472.CAN-10-4610

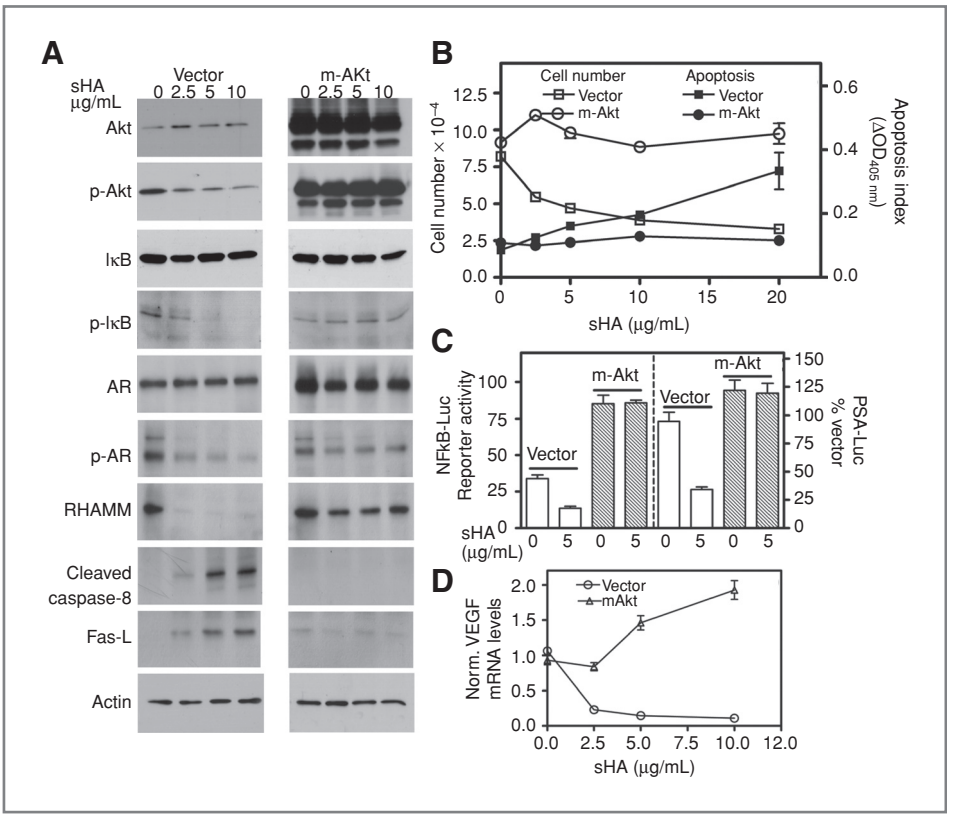

Figure 5. Effect of myr-Akt expression on sHA-induced effects in LNAI cells. LNAI cells were transfected with either vector or myr-Akt plasmid. Twenty-four hours following transfection, cells were treated with sHA for 48 hours. A, immunoblot analysis of vector and myr-Akt transfectants. phospho-Akt, p-Akt; phospho-IκB, p-IκB; phospho-AR, p-AR. B, cell proliferation and apoptosis: following transfection and sHA treatment the cells were counted or subjected to apoptosis measurement. C, NFκB reporter and PSA promoter activities: vector and myr-Akt transfectants of LNAI cells were transfected with pNFκβ-Luc or PSAe1p/Luc plasmids and treated with sHA. The firefly luciferase and *Renilla* luciferase activities were assayed after 24 hours. D, measurement of VEGF mRNA levels by qRT-PCR in vector and myr-Akt transfectants following sHA treatment.

(~100% TUNEL-positive cells), whereas 5% to 10% of cells in the vehicle-treated group were TUNEL positive (Fig. 6D). A tumor specimen from the sHA-treated group had lower MVD than the vehicle-treated group (Fig. 6D). MVD (mean ± SD) from sHA-treated group (1.8 ± 1.5) was approximately 10-fold lower than that in the vehicle-treated group (22.5 ± 6.5; $P < 0.0001$; unpaired t-test).

Discussion

Although HYAL-1 is a critical determinant of tumor growth and metastasis and is an accurate prognostic marker for cancer metastasis, no study so far has targeted HYAL-1 or any other HAase for cancer therapy. The present study not only targets HYAL-1 using a nontoxic HAase inhibitor, sHA, but also delineates the molecular mechanism through which the HA–HAase system might mediate tumor growth and progression. sHA is not a specific inhibitor of HYAL-1 HAase or for prostate cancer cells, rather it inhibits the activity of different HAases by a mixed inhibition mechanism. sHA is also 5-fold more potent in inhibiting HYAL-1 activity than the activity of testicular HAase (7). We have previously shown that unlike acidic HAases (e.g., HYAL-1), HAases, which are active at pH ≥ 5.0 (e.g., testicular), are more resistant to different classes of HAase inhibitors (7). Because HYAL-1 and testicular HAases share about 40% amino acid identity, only the comparison between the crystal structures of sHA bound to HYAL-1 and to testicular HAase can reveal why sHA is more potent in inhibiting HYAL-1 activity; the crystal structure of HYAL-1 has not been deciphered.

The salient features of our study are as follows: (i) sHA inhibits tumor growth mainly by inducing apoptosis via the extrinsic pathway; (ii) sHA is effective in both androgen-dependent and androgen-independent prostate cancer cells; (iii) antitumor, antiangiogenic, and anti-invasive effects of sHA are primarily mediated by the inhibition of PI3K/Akt signaling and transcriptional downregulation of HA receptors; (iv) plausibly, a feedback loop between Akt signaling and HA receptors, controls prostate cancer cell growth, invasion/motility, AR activity, and VEGF production. (v) in xenografts models, sHA is highly effective in inhibiting tumor growth. More than 60% of animals did not form tumors even when the treatment was stopped after a certain period; (Vi) sHA is a potent antiangiogenic agent and causes transcriptional down-regulation of VEGF. With low toxicity, high efficacy, and an easy-to-measure assay for circulating levels, sHA is potentially a promising anticancer agent.

The tumor-associated HA–HAase system plausibly promotes cell survival, proliferation, motility, and invasion and upregulates HA receptor expression by stimulating the PI3K/Akt pathway. By inhibiting the signaling complex between PI3K and HA receptors, sHA inhibits Akt signaling and related events (Supplementary Fig. S6). Because the overexpression of myr-Akt restores the downregulation of HA receptors caused by sHA, inhibition of Akt signaling seems to be responsible for this downregulation. Furthermore, although HA receptor

Published OnlineFirst May 9, 2011; DOI: 10.1158/0008-5472.CAN-10-4610

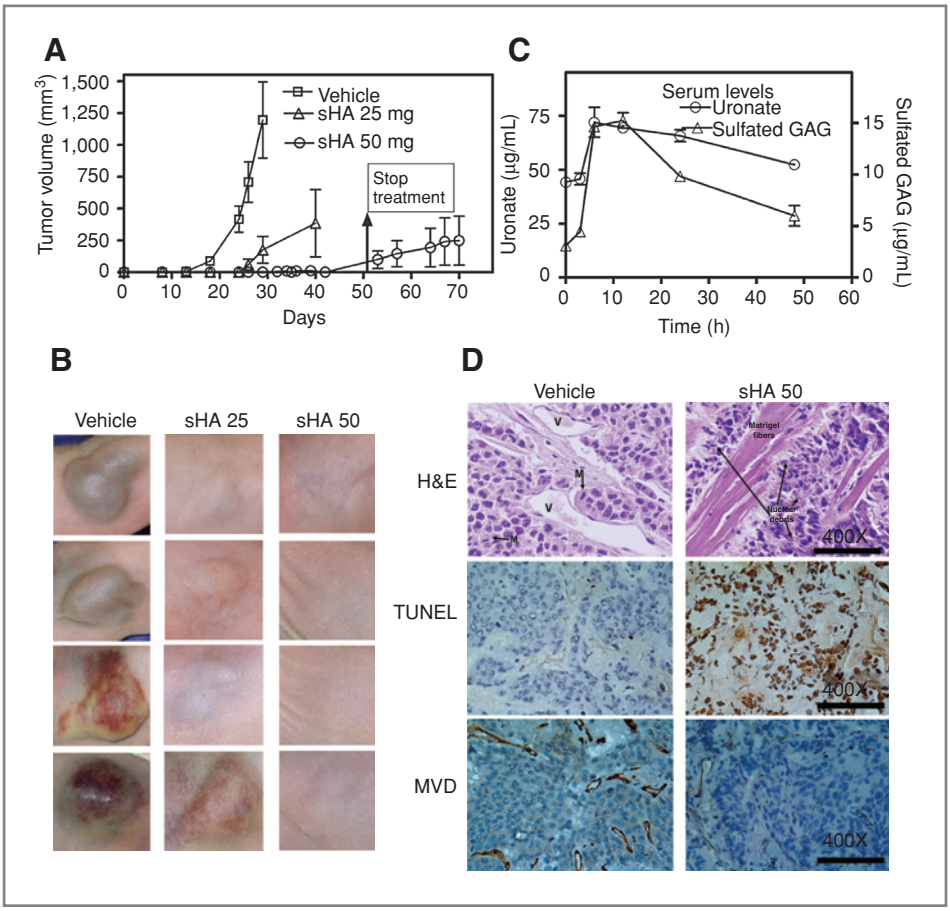

Figure 6. Effect of sHA on LNAI tumor xenografts. A, athymic mice were implanted subcutaneously with LNAI cells and treated twice weekly with vehicle or sHA (25 or 50 mg/kg). In the sHA 50 mg/kg group, for 5 mice, treatment was stopped from day 53 to day 70 and for 1 mouse from day 50 to day 63. B, tumor photographs at day 29 for 3 treatment groups. C, serum total (uronate) and sulfated glycosaminoglycan (GAG) level measurement. Data: mean ± SD. D, hematoxylin–eosin (H&E) staining, TUNEL assay, and MVD determination by immunohistochemistry on paraffin-fixed specimens (vehicle, day 29; sHA 50 mg/kg 40 days). For all panels, magnification is 400×. In the H&E-stained sHA 50 mg/kg specimen, arrows show Matrigel fibers and nuclear debris.

downregulation decreases phosphorylated Akt levels and the overexpression of HA receptors attenuates sHA-mediated inhibition of cell growth, it seems that there is a feedback loop between PI3K/Akt activation and HA receptor expression and the inhibition of this feedback loop is primarily responsible for the antitumor effects of sHA.

Downregulation of HA receptors by sHA is of key importance in shutting down the HA–HAase system. This is because, although the inhibition of HYAL-1 activity will inhibit the generation of angiogenic HA fragment–mediated signaling, in the absence of HAase activity, pericellular HA still can generate intracellular signaling through HA receptors. However, although sHA downregulates both HA receptors, signaling through the HA–HAase system will be inhibited regardless of the presence of pericellular HA. Indeed, more sHA is needed to inhibit cell growth, invasion, motility, and gene expression in DU145 cells, which express both CD44 and RHAMM, than LNAI and LAPC-4 cells, which express only RHAMM. Therefore, sHA plausibly affects 2 interrelated events—inhibition of HAase activity and downregulation of HA receptors.

sHA causes inhibition of Akt phosphorylation as early as 3 hours and it precedes the downregulation of HA receptors and AR phosphorylation. Overexpression of myr-Akt reverses the biological effects of sHA including the inhibition of NFκB reporter activity, AR phosphorylation, and PSA promoter activity. This suggests that downregulation of PI3K/Akt signaling by sHA is the initial event that triggers the inhibition of the feedback loop between Akt and HA receptors leading to induction of apoptosis (49) and the inhibition of VEGF expression, cell motility, and invasion. Inhibition of PI3K/Akt as the initial event may also be the reason why we observed a substantial increase in apoptosis but a modest cell-cycle arrest in sHA-treated cells; the latter would be expected because of the downregulation of RHAMM by sHA (12).

The present study shows that in prostate cancer models, sHA has potent antitumor activity with desirable toxicity profile and ease of detection in serum. In fact, more than 60% of the animals remained tumor free even when the treatment was terminated after a certain period and there was no detectable treatment-related toxicity. Serum-sulfated and total glycosaminoglycan (uronate) levels provide an inexpensive surrogate marker for determining sHA levels in circulation. In addition to prostate cancer, this study will have a broad impact on cancer biology, therapeutics, and the mechanistic understanding of the tumor-associated HA–HAase system; specifically from the standpoint of tumors that express HYAL-1 (e.g., bladder, breast, and prostate) and the HA receptor/Akt-dependent pathways activated in these tumors.

Published OnlineFirst May 9, 2011; DOI: 10.1158/0008-5472.CAN-10-4610

Disclosure of Potential Conflicts of Interest

No potential conflicts of interest were disclosed.

Acknowledgments

We thank Dr. Carlos Perez-Stable, University of Miami, for providing LNAI cells and the PSAe1p/Luc plasmid. We gratefully acknowledge Dr. Eva Turley, London Health Sciences Centre, London, Ontario, Canada, for providing us RHAMM cDNA expression plasmid and Dr. Norman Altman, Department of Pathology, for his help in analyzing tissue histology slides.

Grant Support

This work was supported by grant numbers R01 CA 123063-04 (V.B. Lokeshwar) and R01CA72821-10 (V.B. Lokeshwar).

The costs of publication of this article were defrayed in part by the payment of page charges. This article must therefore be hereby marked *advertisement* in accordance with 18 U.S.C. Section 1734 solely to indicate this fact.

Received December 22, 2010; revised March 29, 2011; accepted April 17, 2011; published OnlineFirst May 9, 2011.

References

1. Simpson MA, Lokeshwar VB. Hyaluronan and hyaluronidase in genitourinary tumors. Front Biosci 2008;13:5664–80.
2. Tammi RH, Kultti A, Kosma VM, Pirinen R, Auvinen P, Tammi MI. Hyaluronan in human tumors: pathobiological and prognostic messages from cell-associated and stromal hyaluronan. Semin Cancer Biol 2008;18:288–95.
3. Ekici S, Cerwinka WH, Duncan R, Gomez P, Civantos F, Soloway MS, et al. Comparison of the prognostic potential of hyaluronic acid, hyaluronidase (HYAL-1), CD44v6 and microvessel density for prostate cancer. Int J Cancer 2004;112:121–9.
4. Posey JT, Soloway MS, Ekici S, Sofer M, Civantos F, Duncan RC, et al. Evaluation of the prognostic potential of hyaluronic acid and hyaluronidase (HYAL1) for prostate cancer. Cancer Res 2003;63:2638–44.
5. Aaltomaa S, Lipponen P, Tammi R, Tammi M, Viitanen J, Kankkunen JP, et al. Strong stromal Hyaluronan expression is associated with PSA recurrence in local prostate cancer. Urol Int 2002;69:266–72.
6. Gomez CS, Gomez P, Knapp J, Jorda M, Soloway MS, Lokeshwar VB. Hyaluronic acid and HYAL-1 in prostate biopsy specimens: predictors of biochemical recurrence. J Urol 2009;182:1350–6.
7. Lokeshwar VB, Rubinowicz D, Schroeder GL, Forgacs E, Minna JD, Block NL, et al. Stromal and epithelial expression of tumor markers hyaluronic acid and HYAL1 hyaluronidase in prostate cancer. J Biol Chem 2001;276:11922–32.
8. Toole BP, Slomiany MG. Hyaluronan: a constitutive regulator of chemoresistance and malignancy in cancer cells. Semin Cancer Biol 2008;18:244–50.
9. Toole BP. Hyaluronan: from extracellular glue to pericellular cue. Nat Rev Cancer 2004;4:528–39.
10. Kobayashi N, Miyoshi S, Mikami T, Koyama H, Kitazawa M, Takeoka M, et. al. Hyaluronan deficiency in tumor stroma impairs macrophage trafficking and tumor neovascularization. Cancer Res 2010;70:7073–83.
11. Itano N, Zhuo L, Kimata K. Impact of the hyaluronan-rich tumor microenvironment on cancer initiation and progression. Cancer Sci 2008;99:1720–5.
12. Maxwell CA, McCarthy J, Turley E. Cell-surface and mitotic-spindle RHAMM: moonlighting or dual oncogenic functions? J Cell Sci 2008;121:925–32.
13. Orian-Rousseau V. CD44, a therapeutic target for metastasising tumours. Eur J Cancer 2010;46:1271–7.
14. Toole BP. Hyaluronan-CD44 interactions in cancer: paradoxes and possibilities. Clin Cancer Res 2009;15:7462–8.
15. Lokeshwar VB, Lopez LE, Munoz D, Chi A, Shirodkar SP, Lokeshwar SD, et al. Antitumor activity of hyaluronic acid synthesis inhibitor 4-methylumbelliferone in prostate cancer cells. Cancer Res 2010;70:2613–23.
16. Lokeshwar VB, Cerwinka WH, Lokeshwar BL. HYAL1 hyaluronidase: a molecular determinant of bladder tumor growth and invasion. Cancer Res 2005;65:2243–50.
17. Lokeshwar VB, Cerwinka WH, Isoyama T, Lokeshwar BL. HYAL1 hyaluronidase in prostate cancer: a tumor promoter and suppressor. Cancer Res 2005;65:7782–9.
18. Bharadwaj AG, Kovar JL, Loughman E, Elowsky C, Oakley GG, Simpson MA. Spontaneous metastasis of prostate cancer is promoted by excess hyaluronan synthesis and processing. Am J Pathol 2009;174:1027–36.
19. Kovar JL, Johnson MA, Volcheck WM, Chen J, Simpson MA. Hyaluronidase expression induces prostate tumor metastasis in an orthotopic mouse model. Am J Pathol 2006;169:1415–26.
20. Kramer MW, Escudero DO, Lokeshwar SD, Golshani R, Ekwenna OO, Acosta K, et al. Association of hyaluronic acid family members (HAS1, HAS2, and HYAL-1) with bladder cancer diagnosis and prognosis. Cancer 2010 Oct 19. [Epub ahead of print].
21. Poola I, Abraham J, Marshalleck JJ, Yue Q, Lokeshwar VB, Bonney G, et al. Molecular risk assessment for breast cancer development in patients with ductal hyperplasias. Clin Cancer Res 2008;15:1274–80.
22. Balazs EA, Hogberg B, Laurent TC. The biological activity of hyaluron sulfuric acid. Acta Physiol Scand 1951;23:168–78.
23. Isoyama T, Thwaites D, Selzer MG, Carey RI, Barbucci R, Lokeshwar VB. Differential selectivity of hyaluronidase inhibitors toward acidic and basic hyaluronidases. Glycobiology 2006;16:11–21.
24. Kunze R, Rösler M, Möller S, Schnabelrauch M, Riemer T, Hempel U, et al. Sulfated hyaluronan derivatives reduce the proliferation rate of primary rat calvarial osteoblasts. Glycoconj J 2010;27:151–8.
25. Ahmed S, Tsuchiya T, Nagahata-Ishiguro M, Sawada R, Banu N, Nagira T. Enhancing action by sulfated hyaluronan on connexin-26, -32, and -43 gene expressions during the culture of normal human astrocytes. J Biomed Mater Res A 2009;90:713–9.
26. Nagira T, Nagahata-Ishiguro M, Tsuchiya T. Effects of sulfated hyaluronan on keratinocyte differentiation and Wnt and Notch gene expression. Biomaterials 2007;28:844–50.
27. Gomez LA, de Las Pozas A, Perez-Stable C. Sequential combination of flavopiridol and docetaxel reduces the levels of X-linked inhibitor of apoptosis and AKT proteins and stimulates apoptosis in human LNCaP prostate cancer cells. Mol Cancer Ther 2006;5:1216–26.
28. Perez-Stable CM, de Las Pozas A, Roos BA. A role for GATA transcription factors in the androgen regulation of the prostate-specific antigen gene enhancer. Mol Cell Endocrinol 2000;167:43–53.
29. Wei DC, Politano VA, Selzer MG, Lokeshwar VB. The association of elevated urinary total to sulfated glycosaminoglycan ratio and high molecular mass hyaluronic acid with interstitial cystitis. J Urol 2000;163:1577–83.
30. Lokeshwar VB, Lokeshwar BL, Pham HT, Block NL. Association of elevated levels of hyaluronidase, a matrix-degrading enzyme, with prostate cancer progression. Cancer Res 1996;56:651–7.
31. Novotny NM, Markel TA, Crisostomo PR, Meldrum DR. Differential IL-6 and VEGF secretion in adult and neonatal mesenchymal stem cells: role of NFkB. Cytokine 2008;43:215–9.
32. Lin HK, Hu YC, Yang L, Altuwaijri S, Chen YT, Kang HY, et al. Suppression versus induction of androgen receptor functions by the phosphatidylinositol 3-kinase/Akt pathway in prostate cancer LNCaP cells with different passage numbers. J Biol Chem 2003;278:50902–7.
33. Li Y, Wang Z, Kong D, Li R, Sarkar SH, Sarkar FH. Regulation of Akt/FOXO3a/ GSK-3beta/AR signaling network by isoflavone in prostate cancer cells. J Biol Chem 2008;283:27707–16.
34. Liu X, Choi RY, Jawad SM, Arnold JT. Androgen-induced PSA expression requires not only activation of AR but also endogenous IGF-I or IGF-I/PI3K/Akt signaling in human prostate cancer epithelial cells. Prostate 2010 Oct 28. [Epub ahead of print].

Published OnlineFirst May 9, 2011; DOI: 10.1158/0008-5472.CAN-10-4610

35. Campo GM, Avenoso A, Campo S, D'Ascola A, Nastasi G, Calatroni A. Small hyaluronan oligosaccharides induce inflammation by engaging both toll-like-4 and CD44 receptors in human chondrocytes. Biochem Pharmacol 2010;80:480–90.
36. Ohno-Nakahara M, Honda K, Tanimoto K, Tanaka N, Doi T, Suzuki A, et al. Induction of CD44 and MMP expression by hyaluronidase treatment of articular chondrocytes. J Biochem 2004;135:567–75.
37. Lokeshwar VB, Selzer MG. Differences in hyaluronic acid-mediated functions and signaling in arterial, microvessel, and vein-derived human endothelial cells. J Biol Chem 2000;275:27641–9.
38. Freedland SJ, Seligson DB, Liu AY, Pantuck AJ, Paik SH, Horvath S, et al. Loss of CD10 (neutral endopeptidase) is a frequent and early event in human prostate cancer. Prostate 2003;55:71–80.
39. Harrison GM, Davies G, Martin TA, Mason MD, Jiang WG. The influence of CD44v3-v10 on adhesion, invasion and MMP-14 expression in prostate cancer cells. Oncol Rep 2006;15:199–206.
40. Liu AY, Brubaker KD, Goo YA, Quinn JE, Kral S, Sorensen CM, et al. Lineage relationship between LNCaP and LNCaP-derived prostate cancer cell lines. Prostate 2004;60:98–108.
41. Lou W, Krill D, Dhir R, Becich MJ, Dong JT, Frierson HF Jr, et al. Methylation of the CD44 metastasis suppressor gene in human prostate cancer. Cancer Res 1999;59:2329–31.
42. Dhir R, Gau JT, Krill D, Bastacky S, Bahnson RR, Cooper DL, et al. CD44 expression in benign and neoplastic human prostates. Mol Diagn 1997;2:197–204.
43. Horiguchi A, Zheng R, Shen R, Nanus DM. Inactivation of the NF2 tumor suppressor protein Merlin in DU145 prostate cancer cells. Prostate 2008;68:975–84.
44. Verkaik NS, Trapman J, Romijn JC, Van Der Kwast TH, Van Steenbrugge GJ. Down-regulation of CD44 expression in human prostatic carcinoma cell lines is correlated with DNA hypermethylation. Int J Cancer 1999;80:439–43.
45. van Bokhoven A, Varella-Garcia M, Korch C, Johannes WU, Smith EE, Miller HL, et al. Molecular characterization of human prostate carcinoma cell lines. Prostate 2003;57:205–25.
46. Ghatak S, Hascall VC, Markwald RR, Misra S. Stromal hyaluronan interaction with epithelial CD44 variants promotes prostate cancer invasiveness by augmenting expression and function of hepatocyte growth factor and androgen receptor. J Biol Chem 2010;285:19821–32.
47. Müller I, Wischnewski F, Pantel K, Schwarzenbach H. Promoter- and cell-specific epigenetic regulation of CD44, cyclin D2, GLIPR1 and PTEN by methyl-CpG binding proteins and histone modifications. BMC Cancer 2010;10:297.
48. van Weering DH, Baas PD, Bos JL. A PCR-based method for the analysis of human CD44 splice products. PCR Methods Appl 1993;3:100–6.
49. Suhara T, Kim HS, Kirshenbaum LA, Walsh K. Suppression of Akt signaling induces Fas ligand expression: involvement of caspase and Jun kinase activation in Akt-medicated Fas ligand regulation. Mol Cell Biol 2002;22:680–91.

Cancer Research
The Journal of Cancer Research (1916–1930) | The American Journal of Cancer (1931–1940)

AACR American Association for Cancer Research

Targeting Hyaluronidase for Cancer Therapy: Antitumor Activity of Sulfated Hyaluronic Acid in Prostate Cancer Cells

Anaid Benitez, Travis J. Yates, Luis E. Lopez, et al.

Cancer Res 2011;71:4085-4095. Published OnlineFirst May 9, 2011.